Structural and Mössbauer characterization of the ball-milled Fe x (Al 2 O 3) 100 x system

A. Paesano Jr., C. K. Matsuda, L. F. Cótica, S. N. de Medeiros, J. B. M. da Cunha, B. Hallouche, and S. L. Silva

Citation: Journal of Applied Physics **96**, 2540 (2004); doi: 10.1063/1.1771480
View online: http://dx.doi.org/10.1063/1.1771480
View Table of Contents: http://scitation.aip.org/content/aip/journal/jap/96/5?ver=pdfcov
Published by the AIP Publishing

Structural and Mössbauer characterization of the ball-milled $Fe_x(Al_2O_3)_{100-x}$ system

A. Paesano, Jr., C. K. Matsuda, L. F. Cótica, and S. N. de Medeiros
Departamento de Física, Universidade Estadual de Maringá, Avenida Colombo 5790, Maringá, Paraná, 87020-900 Brazil

J. B. M. da Cunha
Instituto de Física, Universidade Federal do Rio Grande do Sul, Porto Alegre, Rio Grande do Sul, Brazil

B. Hallouche
Departamento de Química e Física, Universidade de Santa Cruz do Sul, Rio Grande do Sul, Brazil

S. L. Silva
Centro Tecnológico da Marinha, ARAMAR, Iperó, São Paulo, Brazil

(Received 6 January 2004; accepted 19 May 2004)

Metal-oxide composites were synthesized by high-energy ball milling of metallic iron (α-Fe) and alumina (α-Al_2O_3) powders, varying the starting relative concentration and the milling time. The samples were characterized by scanning electron microscopy, x-ray diffraction, and Mössbauer spectroscopy. The results revealed the formation of a $FeAl_2O_{3+W}$ spinel phase (hercynite) and of iron (super)paramagnetic nanoprecipitates, in addition to residual magnetic iron and alumina. We also observed that the relative amounts of nanoprecipitates and hercynite for isochronally milled samples were correlated with the sample nominal concentration x, with the precursor iron being relatively more converted in those phases for low x values. Particularly for $x=10$ milled sample, the relative amounts of the (super)paramagnetic and spinel phases were observed to increase linearly with the milling time. An $x=20/24$ h milled sample was annealed in H_2 atmosphere and revealed the reduction of hercynite, with iron phase separation. © *2004 American Institute of Physics*. [DOI: 10.1063/1.1771480]

I. INTRODUCTION

High-energy ball milling is a powerful method for the synthesis of amorphous and nonequilibrium phases. The reaction obtained from blended metals, oxides or metal-oxide powders is induced by repeated fracturing and welding of the precursors, thus enhancing mechanically the atomic interdiffusion. Nanocrystalline materials can also be prepared by particle size progressive reduction which makes this process important for nanotechnology.

From the thermodynamical point of view, mechanical alloying can add to or remove free energy from the mixture of precursors, depending on milling parameters such as ball-to-powder-mass-ratio, milling energy, milling atmosphere, tribological properties of the vial, and the balls and type of mill, besides, of course, the materials themselves under milling.[1]

High-energy ball milling has been applied to chemical reduction of oxides in systems where the solid state reaction drives spontaneously to the same direction.[2,3] The alumino-mechanical reaction of iron oxides such as hematite and magnetite, for instance, has recently attracted much attention.[1,2,4]

However, since metastable phases with higher free energy than that of the original blend can hypothetically be achieved, one could ask what if a less reactive metal was milled along with a stable oxide made of a more oxygen-reactive metal. To answer this question, we decided to investigate the Fe-Al_2O_3 milled system.

The choice of the system was motivated, first, by the very high stability of the aluminum oxide and the consequent possibility of verifying the mixing ability of the milling process in an extreme case. Additionally, it is also motivating to gain some insight into this system which, not necessarily mixed at atomic level, has potential magnetotransport properties and use as surface coatings by granular films.[5,6]

Until now, the Fe-Al_2O_3 system has already been studied in several basic aspects regarding phase formation, charge state of iron, diffusion, etc. Earlier papers investigated this system when mixed by ion implantation,[7–15] ion beam irradiation,[16–18] hot-pressing,[19] the sol-gel method,[20] and ball milling.[21,22] The magnetic properties of as-deposited and annealed Fe-Al_2O_3 multilayers and of coevaporated granular Fe-Al_2O_3 films have also been intensely investigated.[23–28]

To date, particularly considering the ball-milling process, no systematic investigation of this binary system has been reported. In this sense, in the present study we report results of a structural and Mössbauer investigation carried out on the ball-milled Fe-Al_2O_3 system.

II. EXPERIMENT

$Fe_x(Al_2O_3)_{100-x}$ composites were prepared by high-energy ball milling the mechanical mixture of α-Fe (99.99%) and Al_2O_3 (99.7%) powders, under argon atmosphere, in a SPEX 8000 mill. The precursors were milled in a hardened-steel vial with a tungsten carbide ball and milling times ranging from 1 h to 72 h, with compositions of $x=2$,

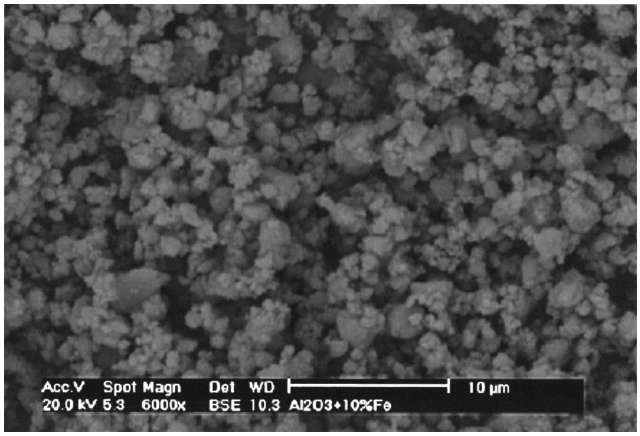

FIG. 1. SEM micrography for the $Fe_{10}(Al_2O_3)_{90}$ as-milled sample.

5, 10, 20, and 60. The ball-to-powder mass ratio was ~4:1. In order to observe the effect of a heat treatment in a reducing atmosphere, a fraction of the $Fe_{20}(Al_2O_3)_{80}$ milled sample was annealed under hydrogen at 1.000 °C for 6 h.

The composites were analyzed by scanning electron microscopy (SEM), x-ray diffraction (XRD), and Mössbauer spectroscopy immediately after the milling process. Scanning electron micrographies were obtained in a Phillips-XL30 microscope. X-ray diffraction measurements were performed using Cu $K\alpha$ radiation ($\lambda = 1.5406$ Å), in a Siemens Diffractometer D500, in the conventional θ-2θ Bragg-Brentano geometry. Mössbauer spectra were taken from a constant acceleration spectrometer with a $^{57}Co(Rh)$ source, using absorbers with nearly 10 mg(Fe)/cm^2. For the low temperature Mössbauer measurements, a Janis (SVT-400) liquid helium cryostat was used.

III. RESULTS AND DISCUSSION

Scanning electron microscopy image of a selected as-milled sample ($x=10$) is shown in Fig. 1. Through the images we can see a flaky material with a homogeneous morphology along the different regions of the powder.

X-ray diffractograms for some representative 24 h milled samples are presented in Fig. 2. The $x=2$ sample pattern (a) reveals only alumina peaks, whereas for $x=20$ (b), the most intense iron peak ($\langle 110 \rangle$) can be clearly identified in the diffractogram. Because of the reduced particle size, defects, and disordering produced during the milling process, the reflection lines of iron and alumina are broadened. However, after heat treatment in H_2 atmosphere [Fig. 2(c)], the lines become narrow and evidently indicate the presence of well-crystallized alumina and iron. For $x=60$ [Fig. 2(d)], a significant change compared to the earlier as-milled sample result may be observed, with a much more intense iron pattern. The fact that peaks belonging to other phases could not be unequivocally identified in these diffractograms is noteworthy.

Figure 3 shows the diffraction patterns for some of the $x=10$ samples milled for different times. Regarding alumina, a complete set of indexed peaks can be identified in all diffractograms, in spite of an increasing broadening of the diffraction lines with the milling time. Diversely, the most in-

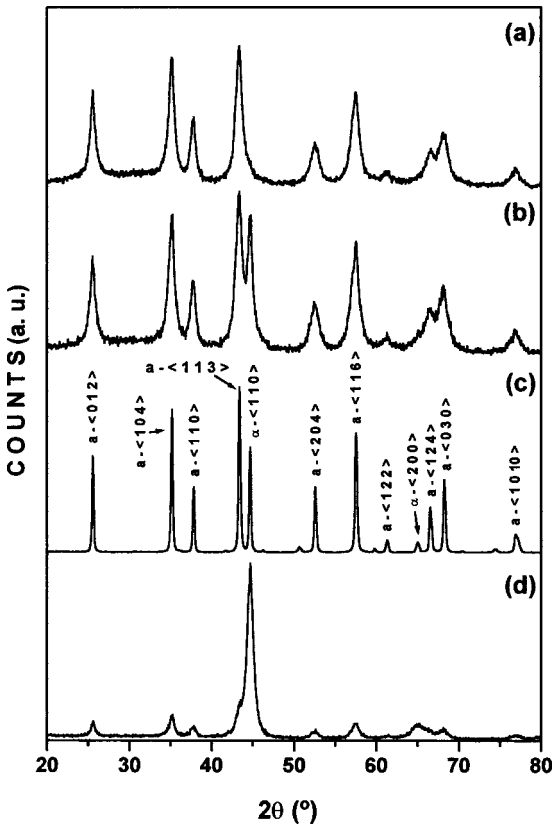

FIG. 2. XRD patterns of 24 h milled samples with $x=2$ (a), 20/as-milled (b) /H_2 annealed (c), and 60 (d). The indexed planes belonging to the α-Fe and α-Al_2O3 phases are identified by α and a, respectively.

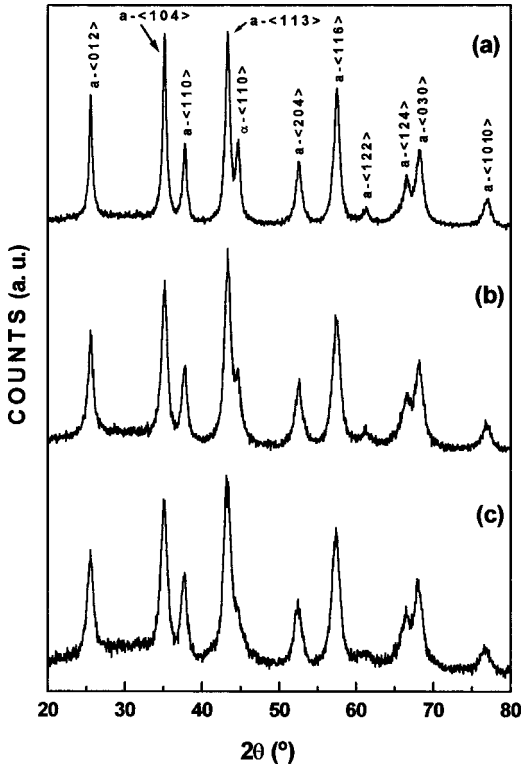

FIG. 3. XRD patterns of the $x=10$ samples milled for 6 h (a), 12 h (b) and 72 h (c). The indexed planes belonging to the α-Fe and α-Al_2O_3 phases are identified by α and a, respectively.

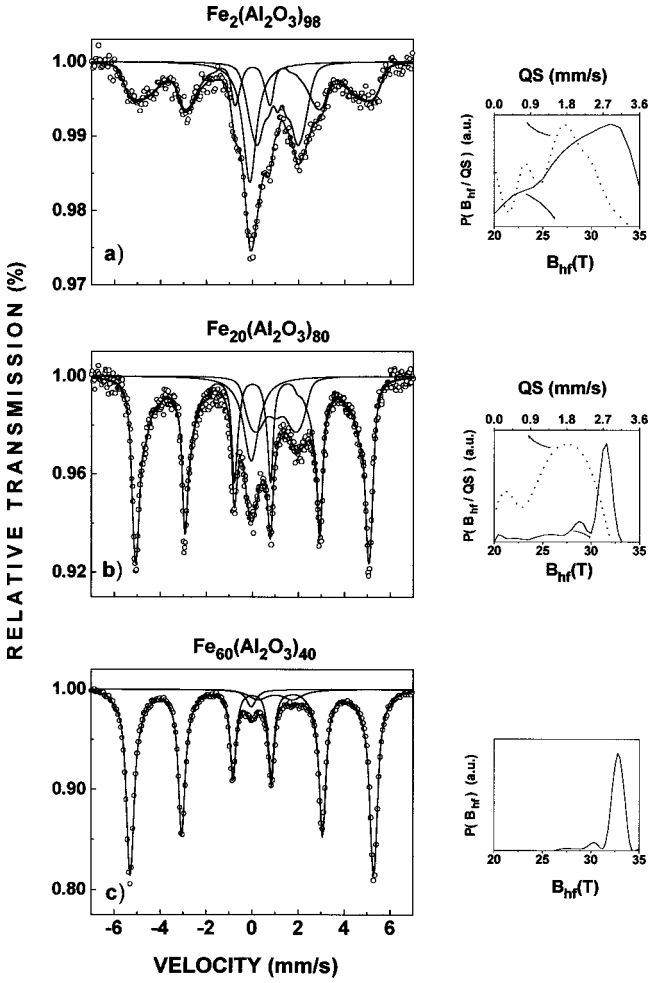

FIG. 4. Mössbauer spectra of the 24 h milled samples with $x=2$ (a), 20 (b) and 60 (c), measured at RT, with the respective B_{hf} (continuous line) and QS (dotted line) distributions.

tense iron peak is well resolved only for the milling shortest time (6 h) but it is reduced just to a shoulder when the milling time is extended to 72 h.

Mössbauer results of some selected samples, milled for 24 h, are shown in Fig. 4. These spectra are similar to those obtained from arc-melted samples.[29] In the present cases, they were fitted using a magnetic hyperfine field (B_{hf}) distribution, a quadrupolar splitting (QS) distribution, and a singlet. Both distributions are shown as insets in the figure. For the $x=60$ spectrum only, a discrete QS component was employed. The hyperfine parameters and the relative areas of the subspectra for all measured samples are displayed in Table I.

The QS distributions for the 24 h ball-milled samples, although not absolutely identical to those of the arc-melted hercynite, have shapes with average QS and isomer shift (IS) values comparable to those obtained from the previously synthesized standard. Analogously, the spectra in Fig. 5 for a series of isoconcentration samples, reveal QS distributions and IS equally consistent with our reference pattern. Based on these evidences and on previous Mössbauer data reported in the literature, we attribute the QS component to the hercynite phase ($FeAl_2O_4$) in spite of some contradiction in the earlier results on account of different methods of sample preparation.[30–39] The absence of the lines respective to this spinel structure in our x-ray diffractograms may be attributed to the size of the hercynite grains that are probably too small to be seen by XRD.

Hercynite is a spinel belonging to a cubic oxide class usually denoted by AB_2O_4, where the A and B sites have tetrahedral and octahedral symmetries, respectively.[30] In the "normal" state, hercynite should have only Fe^{+2} ions at A sites and Al^{+3} at B sites. However, a small difference among the site energies causes some of the Fe^{+2} ions to be found at octahedral B sites in $FeAl_2O_4$ (and, of course, Al^{+3} at A sites) giving a partially inverse cation distribution represented by $Fe^{+2}{}_{1-\xi}Al^{+3}{}_{\xi}[Fe^{+2}{}_{\xi}Al^{+3}{}_{2-\xi}]O_4$, where ξ represents the degree of inversion and can have values between 0 (normal state) and 1 (inverse state).[31–33] The inversion originates a variety of neighborhoods for the iron in both sites. For this reason, as in our previous study with arc-melted Fe-Al_2O_3 samples, we tried here to fit the quadrupolar component using a number of discrete subspectra. The fittings obtained resulted in subspectra having quadrupolar splittings and (large) linewidths very dependent on the configuration of initial parameters, although invariably showing close values for IS. The ambiguities related to the quadrupolar components indicate a complex iron surrounding configuration and the small difference between the IS of A and B sites may be explained by the similar bond distances in the two types of sites.[38] Hence, we took the hercynite quadrupolar contribution into account by using a QS distribution (histogram) with a single IS for every component, and we proceeded in the same way with the arc-melted hercynite samples.[29]

Similarly to the spectra of samples prepared in arc furnace, it was not possible to superimpose any Fe^{+3} doublet spectrum, albeit some authors have observed the presence of iron trivalent in hercynite containing samples.[3] Therefore, the present Mössbauer results demonstrate that we have a very low content of ferric ion, if any, in agreement with the idea that hercynite does not show ferric ions at either tetrahedral or octahedral sites.[32]

Although the hyperfine parameters (IS and QS) found in the present investigation for the spinel are consistent with those determined by other authors, the hercynite formation cannot be interpreted in a straightforward manner. Usually, the reaction assumed for hercynite formation is $FeO + Al_2O_3 > FeAl_2O_4$.[39] However, in the present study, as in the previous one we conducted using Fe-Al_2O_3 arc-melted samples, there are no available sources of free oxygen for the reaction with iron dissolved in alumina. For this reason, we suggest that the iron dissolved in alumina by mechanical action in the milling process forms hercynite with oxygen vacancies, i.e., $FeAl_2O_{3+W}$ $(0 \leqslant W \leqslant 1)$. Actually, the occurrence of this defective oxide has already been identified for iron implanted in sintered alumina.[10]

On the other hand, the magnetic spectral component is attributed to the nonmixed or unreacted α-Fe on which the particle size reduction induced by the milling process produces relaxation effects which are visible in the Mössbauer lines. In fact, the milling process is expected to cause a size decrease in the grains until they reach a volume distribution

TABLE I. Mössbauer hyperfine parameters and subspectral areas for the $Fe_x(Al_2O_3)_{100-x}$ milled samples.

Fe starting concentration (x)	Milling time (h)	Subspectrum	δ[a] (mm/s) (±0.01)	ΔE_Q[b] (mm/s) (±0.02)	B_{hf}[c] (kOe) (±3)	Γ[d] (mm/s)	Area (%) (±0.1)
		B_{hf} dist	−0.01	⋯	292	⋯	48.2
2	24	QS dist	1.09	1.67	⋯	⋯	31.2
		Singlet	−0.11	⋯	⋯	0.70	20.6
		B_{hf} dist	−0.01	⋯	318	⋯	61.4
5	24	QS dist	1.13	1.56	⋯	⋯	21.0
		Singlet	−0.12	⋯	⋯	0.71	17.6
		B_{hf} dist	0.00	⋯	328	⋯	83.7
10	6	Doublet	1.14	1.66	⋯	1.03	11.0
		Singlet	−0.09	⋯	⋯	0.55	5.3
		B_{hf} dist	0.00	⋯	326	⋯	77.6
10	12	Doublet	1.07	1.70	⋯	1.04	16.0
		Singlet	−0.09	⋯	⋯	0.61	6.4
		B_{hf} dist	−0.01	0.00	301	⋯	61.4
10	24	QS dist	1.26	1.34	⋯	⋯	15.3
		Singlet	−0.09	⋯	⋯	0.76	23.3
		B_{hf} dist	0.00	⋯	311	⋯	49.4
10	48	QS dist	1.16	1.45	⋯	⋯	24.2
		Singlet	−0.11	⋯	⋯	0.74	26.4
		B_{hf} dist	−0.01	⋯	284	⋯	32.1
10	72	QS dist	1.23	1.46	⋯	⋯	30.9
		Singlet	−0.10	⋯	⋯	0.76	37.0
		B_{hf} dist	0.01	⋯	298	⋯	69.2
20	24	QS dist	1.01	1.49	⋯	⋯	17.9
		Singlet	−0.05	⋯	⋯	0.80	12.9
20[e]	24	B_{hf}	0.01	⋯	315	0.25	79.3
		Singlet	−0.08	⋯	⋯	0.31	20.7
20[e,f]	24	B_{hf}	0.11	⋯	336	0.28	80.0
		Singlet	−0.03	⋯	⋯	0.80	20.0
		B_{hf} dist	−0.01	⋯	325	⋯	91.7
60	24	Dublet	1.01	1.50	⋯	1.00	5.7
		Singlet	−0.03	⋯	⋯	0.50	2.6

[a]Relative to α-Fe foil at room temperature.
[b]Average quadrupole splitting, in case of distribution.
[c]Average hyperfine magnetic field, in case of distribution.
[d]The linewidth used in the distributions varied between 0.27 and 0.30 mm/s.
[e]H_2 annealed.
[f]Measured at 5.3 K.

in nanometer scale. Eventually, some fraction of particles will have a volume smaller than the blocking one, when they will present a superparamagnetic behavior, which would be evidenced by a singlet, as that single line component always present in the spectra of Fe-Al_2O_3 milled samples for every nominal concentration. In line with the above arguments, this contribution (i.e., the singlet) could be attributed to iron in superparamagnetic nanoprecipitates, which may or may not have some aluminum content dissolved in them (see Discussion ahead). Depending on the aluminum content, the nanoprecipitates can simply be paramagnetic, according to the magnetic phase diagram of the system.[40] It must also be stressed that, from the morphological point of view, we cannot disregard the possibility that this magnetically nonordered phase might be disposed at the surface of an ordered iron-aluminum core as a thin layer (i.e., a shell), where surface energy effects have disarranged the spins. In any case, however, we have to consider that the single line component is a consequence of the presence of a peculiar nanoscaled structure.

Several authors have observed this singlet given that a single line with similar values for the IS has been reported for iron implanted alumina samples and as-sputtered Fe:Al_2O_3 thin films.[7,8,10–12,28] We have detected this pattern in Fe-Al_2O_3 arc-melted samples as well.[29] However, complete agreement is not there on the interpretation of this phase, since both superparamagnetic α-Fe and stabilized γ-Fe have been identified as causing this nonmagnetic contribution.

Aiming to analyze the influence of the milling time, the spectra of an $x=10$ series of samples milled by different periods are displayed in Fig. 5. The same earlier types of subspectral components were used to fit these spectra. It can be seen that, for 12 h of milling [Fig. 5(a)], most of the iron remained unreacted and in a magnetic state. For longer millings [Figs. 5(b) and 5(c)], the iron shows again magnetic relaxation resulting from the particle size reduction, as revealed by the broadening of the sextet lines.

The subspectral areas as a function of concentration, x, for isochronally samples milled (i.e., 24 h), are plotted in

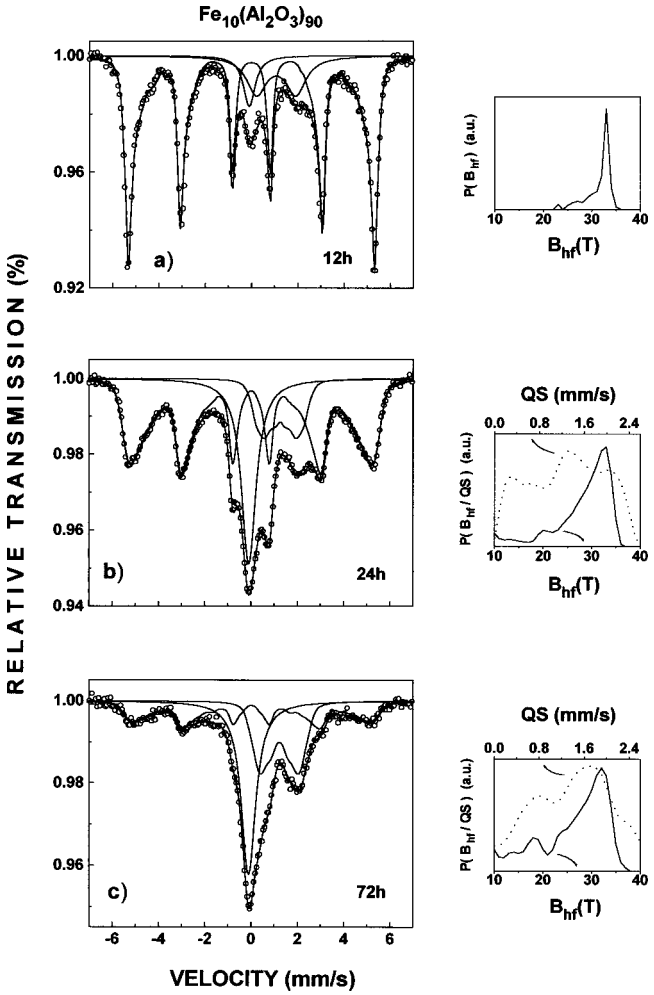

FIG. 5. Mössbauer spectra of the $x=10$ samples milled for 12 h (a), 24 h (b) and 72 h (c), measured at RT, with the respective B_{hf} (continuous line) and QS (dotted line) distributions.

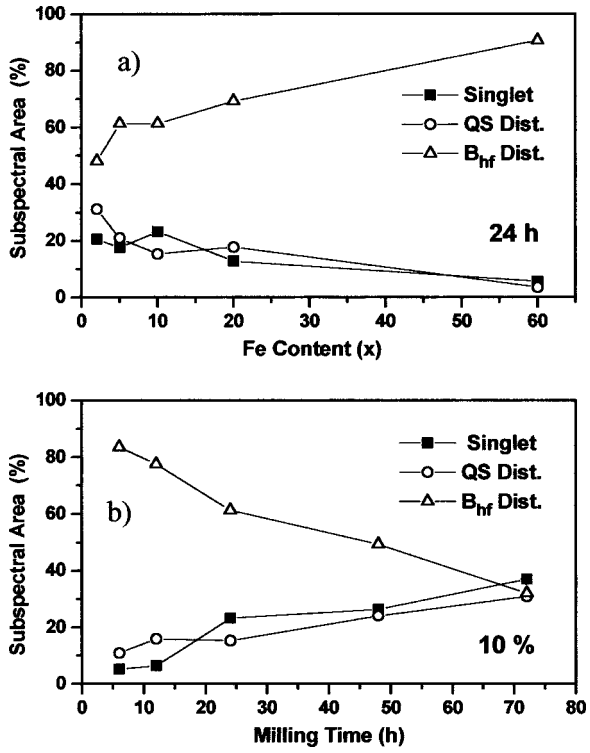

FIG. 6. Mössbauer subspectral areas of the magnetic, quadrupolar and single line components of samples milled for 24 h, as a function of concentration x (a), and for $x=10$ milled samples, as a function of the milling time (b).

Fig. 6(a). The amount of residual magnetic α-Fe grows monotonically, approaching 100% at higher iron concentrations, whereas the single line component shows an apparent maximum at $x=10$ and then falls with increasing sample nominal concentration. Likewise, the hercynite subspectrum area reduces its contribution from the lowest starting iron content up to the highest one. This behavior reveals that a more effective fractional conversion of precursor iron in the mixed oxide takes place at the lowest iron concentrations.

The subspectral areas were also plotted as a function of milling time for the samples with concentration $x=10$, as shown in Fig. 6(b). It is observed that the area of the magnetic distribution decreases whereas the quadrupolar and the singlet components increase with the milling time, all of which roughly linearly. It is worth noting how the metallic (super)paramagnetic nanoprecipitates and hercynite present nearly the same transformed fraction varying either the concentration or the milling time. This allows us to equate the reaction for $x=10$, for any milling time, and assuming (i) no oxygen loss and (ii) similar f factors for both phases by the equation:

$$0.1\mathrm{Fe} + 0.9\mathrm{Al_2O_3} \Rightarrow (0.1-2Z)\,.\,\mathrm{Fe}_{mag} + Z\,.\,\mathrm{Fe}_{(s)pm} + Z\,.\,\mathrm{Fe}_{(s)pm} + Z\,.\,\mathrm{FeAl_2O_{3+W}} + \left[0.9 - \frac{Z}{3}(3+W)\right].\,\mathrm{Al_2O_3} + \left(\frac{2ZW}{3}\right).\,\mathrm{Al}$$

where Z is the molar fraction of (super)paramagnetic iron or, still, of hercynite and W accounts for the oxygen stoichiometry of hercynite, as pointed out above. Obviously, Z depends on the milling time and has the conceivable limit value of 0.05 for $x=10$.

Through the fifth term on the right side of the above equation, we see that an amount of free aluminum could hypothetically be available to react with iron forming, depending on W, a compound or a solid solution of Fe-Al (magnetic or not). Examining the two limit cases, we see that if the reacted hercynite is stoichiometric (i.e., if $W=1$), even a nonmagnetic nanometric alloy of the type $Fe_{60}Al_{40}$ could be produced through milling, in the limit for long milling times. However, if hercynite is deficient in one atom of oxygen (i.e., if $W=0$), the singlet as well as the sextet can be attributed to elemental iron which has a grain size distribution. However, in our opinion, the most probably occurring situation is the intermediary case of a solid solution of iron with some dissolved aluminum [i.e., Fe (Al)].

The RT and 5.3 K spectra for the $x=20/24$ h milled and H_2 annealed sample are shown in Fig. 7. Diversely from the

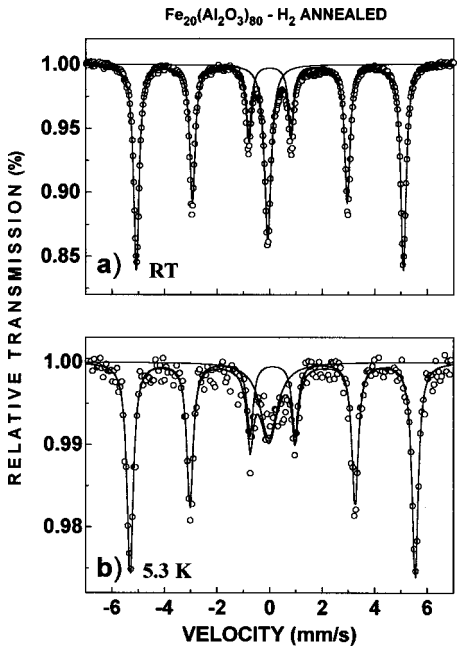

FIG. 7. Mössbauer spectra of the $x=20/24$ h milled and H_2 annealed sample measured at RT (a) and measured at 5.3 K (b).

as-milled sample [Fig. 4(b)], the spectra for the treated sample were fitted with only two components, a discrete sextet and a singlet, which means that hercynite is not present anymore. This is a result of the chemical reduction of the spinel by hydrogen, which implied a phase separation of iron and alumina. The separated iron was shared between the magnetic and the (super)paramagnetic iron phases (see Table I). Comparing the iron lines of this sample with those of the as-milled one, the better crystallization of the metallic phases is clearly shown. In spite of this, the hyperfine magnetic field of the iron sextet decreased ~5% compared to the reference value, suggesting the presence of aluminum also in the magnetic iron lattice. The spectrum in Fig. 7(b) shows that the singlet became broadened but the relative areas of both components did not significantly change (see Table I). This does not corroborate the proposition that the singlet found at RT belongs to an α-Fe(Al) phase, in which relaxation effects due to the small particle size have annulled the effective hyperfine magnetic field. If that were the case, it would be expected that by decreasing the temperature of the superparamagnetic sample, the relaxation time would increase, thus recovering the magnetic splitting of the respective subspectral component. At this time, either a paramagnetic α phase or a metastabilized γ-Fe(Al) phase, both disregarded by us when characterizing arc-melted samples, have to be reconsidered as causing this commonly observed singlet. In order to get additional information about the system, Mössbauer experiments with an external applied magnetic field are currently being conducted.

IV. CONCLUSIONS

We successfully prepared $Fe_x(Al_2O_3)_{100-x}$ nanocomposites by high-energy ball milling of iron and alumina powders. The characterization analyses revealed, as a result of milling, the particle size reduction of the precursors, iron and alumina, and the mecanosynthesis of hercynite. In addition, the Mössbauer spectroscopy showed that the iron is partially left in the form of magnetically nonaligned nanoprecipitates. The relative transformed amounts of this (super)paramagnetic iron and of the hercynite depend on the sample nominal starting concentration x. The hercynite fraction decreases with increasing x for milled samples, which show a maximum for the (super)paramagnetic phase formation in samples with $x=10$. For this composition, the milling process leads the fractions of (super)paramagnetic nanoprecipitates and hercynite to increase with the milling time roughly linearly and at the same rate, at the expense of the precursor magnetic iron.

ACKNOWLEDGMENTS

We greatly appreciate the financial support from the Brazilian agencies CAPES (PROCAD), FUNDAÇÃO ARAUCÁRIA, and FAPERGS.

[1] C. Suryanarayana, Prog. Mater. Sci. **46**, 1 (2001); and references therein.
[2] L. Takacs, Nanostruct. Mater. **2**, 241 (1993).
[3] P. M. Botta, R. C. Mercader, E. F. Aglietti, and J. M. Porto López, Scr. Mater. **48**, 1093 (2003).
[4] L. Takacs, Mater. Lett. **13**, 119 (1992).
[5] M. A. S. Boff, J. Geshev, J. E. Schmidt, W. H. Flores, A. B. Antunes, M. Gusmão, and S. R. Teixeira, J. Appl. Phys. **91**, 9909 (2002).
[6] T. Zhu, Y. J. Wang, H. W. Zhao, J. G. Zhao, and W. S. Zhan, J. Appl. Phys. **89**, 6877 (2001).
[7] C. J. McHargue, G. C. Farlow, P. S. Sklad, C. W. White, A. Perez, N. Kornilios, and G. Marest, Nucl. Instrum. Methods Phys. Res. B **19/20**, 813 (1987).
[8] C. Donnet, H. Jaffrezic, G. Marest, N. Moncoffre, and J. Tousset, Nucl. Instrum. Methods Phys. Res. B **50**, 410 (1990).
[9] G. Marest, C. Donnet, N. Moncoffre, and J. Tousset, Hyperfine Interact. **56**, 1613 (1990).
[10] C. Donnet, G. Marest, N. Moncoffre, and J. Tousset, Nucl. Instrum. Methods Phys. Res. B **59/60**, 1177 (1991).
[11] C. J. McHargue, P. S. Sklad, C. W. White, G. C. Farlow, A. Perez, and G. Marest, J. Mater. Res. **6**, 2145 (1991)
[12] C. J. McHargue, P. S. Sklad, C. W. White, J. C. McCallum, A. Perez, and G. Marest, J. Mater. Res. **6**, 2160 (1991).
[13] F. Thimon, G. Marest, and N. Moncroffre, Thin Solid Films **237**, 208 (1994).
[14] C. J. McHargue, S. X. Ren, P. S. Sklad, L. F. Allard, and J. Hunn, Nucl. Instrum. Methods Phys. Res. B **116**, 173 (1996).
[15] T. Kobayashi, A. Nakanishi, K. Fukumura, and G. Langouche, J. Appl. Phys. **83**, 4631 (1998).
[16] S. B. Ogale, D. M. Phase, P. P. Patil, S. M. Kanetkar, S. V. Ghaisas, V. G. Bhide, and S. K. Date, Hyperfine Interact. **29**, 1193 (1986).
[17] A. Perez, E. Abonneau, G. Fuchs, M. Treilleux, C. J. McHargue, and D. L. Joslin, Nucl. Instrum. Methods Phys. Res. B **65**, 129 (1992).
[18] S. K. Sinha, D. C. Kothari, K. M. Vigen, T. Som, V. N. Kulkarni, S. Panchapakesan, and K. G. M. Nair, Nucl. Instrum. Methods Phys. Res. B **159**, 227 (1999).
[19] Epicier, C. Esnouf, M. A. Smith, and D. Pope, Philos. Mag. Lett. **65**, 299 (1992).
[20] A. Santos, J. D. Ardisson, A. D. C. Viegas, J. E. Schmidt, A. I. C. Persiano, and W. A. A. Macedo, J. Magn. Magn. Mater. **226–230**, 1861 (2001).
[21] A. K. Giri, MRS Bull. **32**, 523 (1997).
[22] P. Matteazzi, and M. Alcalà, Mater. Sci. Eng., A **230**, 161 (1997).
[23] J. L. Dormann, C. Djega-Mariadassou, and P. Renaudin, Hyperfine Interact. **56**, 1683 (1990).
[24] O. Lenoble, Ph. Bauer, J. F. Bobo, H. Fischer, M. F. Ravet, and M. Piecuch, J. Phys.: Condens. Matter **6**, 3337 (1994).
[25] O. Lenoble, J. F. Bobo, L. Hennet, H. Fischer, Ph. Bauer, and M. Piecuch, Thin Solid Films **275**, 64 (1996).
[26] S. R. Teixeira, M. A. S. Boff, W. H. Flores, J. E. Schmidt, M. C. M. Alves, and H. C. N. Tolentino, J. Magn. Magn. Mater. **233**, 96 (2001).

[27]N. M. Dempsey, L. Ranno, D. Givord, J. Gonzalo, R. Serna, G. T. Fei, A. K. Petford-Long, R. C. Doole, and D. E. Hole, J. Appl. Phys. **90**, 6268 (2001).
[28]F. Thimon, G. Marest, and N. Moncroffre, Nucl. Instrum. Methods Phys. Res. B **80/81**, 1241 (1993).
[29]A. Paesano, Jr., C. K. Matsuda, J. B. M. da Cunha, M. A. Z. Vasconcellos, B. Hallouche, and S. L. Silva, J. Magn. Magn. Mater. **264**, 264 (2003).
[30]H. B. Mathur, A. P. B. Sinha, and C. M. Yagnik, Indian J. Pure Appl. Phys. **5**, 155 (1967).
[31]C. M. Yagnik, and H. B. Mathur, J. Phys. C **1**, 469 (1968).
[32]G. Dehe, B. Seidel, K. Melzer, and C. Michalk, Phys. Status Solidi A **31**, 439 (1975).
[33]L. Larsson, H. ST. O'Neill, and H. Annersten, Eur. J. Mineral. **6**, 39 (1994).
[34]T. Mizoguchi and M. Tanaka, J. Phys. Soc. Jpn. **18**, 1301 (1963).
[35]M. J. Rossiter, J. Phys. Chem. Solids **26**, 775 (1965).
[36]K. Ono, A. Ito, and Y. Syono, Phys. Lett. **19**, 620 (1966).
[37]G. M. Bancroft, M. D. Osborne, and M. E. Fleet, Solid State Commun. **47**, 623 (1983).
[38]R. J. Hill, Am. Mineral. **69**, 937 (1984).
[39]G. Marest, N. Moncoffre, F. Thimon, M. Brunel, and C. Esnouf, Hyperfine Interact. **92**, 1303 (1994).
[40]O. Kubaschewski, *Binary Phase Diagrams* (Springer, New York, 1982).